(12) INTERNATIONAL APPLICATION PUBLISHED UNDER THE PATENT COOPERATION TREATY (PCT)

(19) World Intellectual Property Organization
International Bureau

(43) International Publication Date
12 September 2019 (12.09.2019)

WIPO | PCT

(10) International Publication Number
WO 2019/169455 A1

(51) International Patent Classification:
G06N 3/02 (2006.01) *A61N 5/00* (2006.01)
G06T 7/73 (2017.01) *A61B 6/00* (2006.01)

(21) International Application Number:
PCT/AU2019/050212

(22) International Filing Date:
08 March 2019 (08.03.2019)

(25) Filing Language: English

(26) Publication Language: English

(30) Priority Data:
2018900755 08 March 2018 (08.03.2018) AU

(72) Inventors; and
(71) Applicants: **NGUYEN, Doan Trang** [AU/AU]; 4/19 Meadow Crescent, Meadowbank, New South Wales 2114 (AU). **KEALL, Paul** [AU/AU]; 9 Landsdowne Street, Greenwich, New South Wales 2065 (AU). **MYLONAS, Adam** [AU/AU]; 121 Chapel Lane, Baulkham Hills, New South Wales 2153 (AU).

(74) Agent: **FPA PATENT ATTORNEYS PTY LTD**; Level 43, 101 Collins Street, Melbourne, Victoria 3000 (AU).

(81) Designated States *(unless otherwise indicated, for every kind of national protection available)*: AE, AG, AL, AM, AO, AT, AU, AZ, BA, BB, BG, BH, BN, BR, BW, BY, BZ, CA, CH, CL, CN, CO, CR, CU, CZ, DE, DJ, DK, DM, DO, DZ, EC, EE, EG, ES, FI, GB, GD, GE, GH, GM, GT, HN, HR, HU, ID, IL, IN, IR, IS, JO, JP, KE, KG, KH, KN, KP, KR, KW, KZ, LA, LC, LK, LR, LS, LU, LY, MA, MD, ME, MG, MK, MN, MW, MX, MY, MZ, NA, NG, NI, NO, NZ, OM, PA, PE, PG, PH, PL, PT, QA, RO, RS, RU, RW, SA, SC, SD, SE, SG, SK, SL, SM, ST, SV, SY, TH, TJ, TM, TN, TR, TT, TZ, UA, UG, US, UZ, VC, VN, ZA, ZM, ZW.

(84) Designated States *(unless otherwise indicated, for every kind of regional protection available)*: ARIPO (BW, GH, GM, KE, LR, LS, MW, MZ, NA, RW, SD, SL, ST, SZ, TZ, UG, ZM, ZW), Eurasian (AM, AZ, BY, KG, KZ, RU, TJ, TM), European (AL, AT, BE, BG, CH, CY, CZ, DE, DK, EE, ES, FI, FR, GB, GR, HR, HU, IE, IS, IT, LT, LU, LV, MC, MK, MT, NL, NO, PL, PT, RO, RS, SE, SI, SK, SM, TR), OAPI (BF, BJ, CF, CG, CI, CM, GA, GN, GQ, GW, KM, ML, MR, NE, SN, TD, TG).

Published:
— *with international search report (Art. 21(3))*

(54) **Title:** METHOD AND SYSTEM FOR GUIDED RADIATION THERAPY

(57) **Abstract:** The present invention is concerned with a method and system for guiding a radiation therapy system. The method comprises: capturing an image of a target area to which radiation is to be delivered; analysing the image with a trained convolutional neural network to determine the position of one or more objects of interest present in the target area; and outputting the determined position/s to the radiation therapy system.

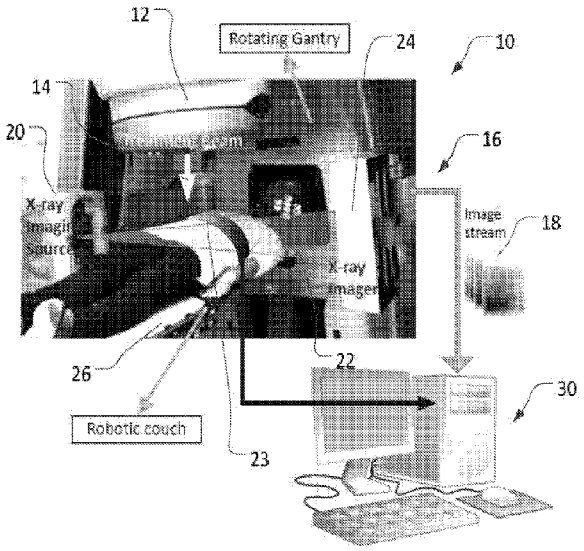

FIGURE 1

WO 2019/169455 A1

Method and system for guided radiation therapy

Field of the invention

The present disclosure relates to methods and systems for use in relation to guided radiation therapy systems. In one form, there is disclosed a method and system for guiding a radiation therapy system by reference to the position of fiducial markers implanted in the tumour that is to be radiated.

Background of the invention

Radiation therapy is a treatment modality used to treat localised tumours. It generally involves producing high energy megavoltage (MV) and conformal beams of x-rays to the target (tumour) using a medical linear accelerator. The radiation interacts with the tissues to create double strand DNA breaks to kill tumour cells. Radiation therapy requires high precision to deliver the dose to the tumour and spare healthy tissue, particularly that of organs surrounding the tumour. Each treatment is tailored to the individual patient.

Advances in radiation therapy techniques, such as intensity modulated radiation therapy (IMRT) and image guided radiation therapy (IGRT) have resulted in improved delivery of radiation doses to tumours while reducing normal tissue toxicity. According to current practices, IGRT is routinely applied at the start of treatment to align the target with its planned position. However, tumours in the thorax, abdomen and pelvis are not static during treatment; a phenomenon known as 'intrafraction motion'. Intrafraction motion occurs when patients move while on the treatment bed (both during setup and treatment) or when organs and tumours move in response to breathing. Real-time image guided adaptive radiation therapy (IGART) systems have been developed at least in part to account for this intrafraction motion.

Certain IGRT and IGART systems operate in real-time by utilising kilovoltage (kV) images for the tracking of fiducial markers implanted in tumours. One such system is known as Kilovoltage Intrafraction Monitoring (KIM). KIM is a real-time image guidance technique that utilises existing radiotherapy technologies found in cancer care centres (i.e. on-board x-ray images). KIM exploits fiducial markers implanted inside the tumour (organ) and reconstructs their location by acquiring multiple images of the target using the on-board kilovoltage (KV) beam (which is a low energy X-ray imager) and determining any motion in the left-right (LR),

superior-inferior (SI), and anterior-posterior (AP) directions. KIM Tracking has also been developed, which dynamically modifies the position of a multi leaf collimator (MLC) while delivering the treatment dose based on the tumour position reconstructed by KIM. In KIM, tumour motion is monitored in real-time while both the MV beam is delivering the treatment dose, and the KV beam is imaging the tumour target. If significant motion away from the treatment beam occurs, the treatment is paused and the patient is repositioned before the treatment is continued.

Such real-time IGRT systems typically require accurate segmentation methods to detect and track the fiducial markers, with these methods currently being based on the approach of 'template matching'. Template matching involves detecting a marker in an image by the use of a template image that represents the marker (Campbell *et. al.* 2017. *Automated target tracking in kilovoltage images using dynamic templates of fiducial marker clusters*, Medical Physics 44 364-374) In turn, the template of a marker is typically based upon *a priori* knowledge of the marker properties (e.g its shape and size). Typically for regular shaped markers (eg spherical and cylindrical gold), templates are built based on known properties of the marker such as dimensions. Other types of markers such as coiled markers (e.g Visicoil™ and IBA Dosimetry) can be used to decrease migration, however, they are subject to deformation into an arbitrary shape upon implantation resulting in unknown marker properties. In these circumstances, an additional learning period is required to determine the marker properties and develop a template.

While methods are being developed to automatically produce templates without such *a priori* knowledge, (Fledelius, 2011, *et al*, *Robust automatic segmentation of multiple implanted cylindrical gold fiducial markers in cone-beam CT projections.* Medical Physics 38. 6351-6361; Poulsen et al 2011, Bertholet et at. 2017), these require this additional learning period during which the marker orientation is learned on the fly. Having a learning period runs the risk of the patient receiving unnecessary radiation.

In addition, many CT images have insufficient resolution and include metal artefacts from the markers. As such, templates typically cannot be constructed prior to treatment, but are instead usually generated online before the time of MV beam-on. For arbitrarily shaped markers, four to five projections with reasonable angular separation are typically required to generate the requisite template. As noted above, this learning period has the drawback of subjecting a patient to unnecessary radiation, namely that delivered to the patient for the purpose of imaging.

The present invention aims to provide an alternative approach to segmentation for use in real-time systems.

Reference to any prior art in the specification is not an acknowledgment or suggestion that this prior art forms part of the common general knowledge in any jurisdiction or that this prior art could reasonably be expected to be understood, regarded as relevant, and/or combined with other pieces of prior art by a skilled person in the art.

Summary of the invention

In a first aspect there is provided a method for guiding a radiation therapy system, comprising:

capturing an image of a target area to which radiation is to be delivered;

analysing the image with a trained convolutional neural network to determine the position of one or more objects of interest present in the target area; and

outputting the determined position/s to the radiation therapy system.

At least in preferred embodiments, the present invention is concerned with a radiation therapy control system that utilises a deep learning convolutional neural network (CNN) to classify objects of interest (such as fiducial markers in kV images) and thereby determine their position. More specifically, the present invention includes the training of a CNN (typically conducted using images of an anthropomorphic phantom and previous images) to initially differentiate between 'marker' and 'background' regions of the image. The thus trained CNN is then utilised in a tracking system to efficiently track the position of the object of interest in a series of images, in close to or in real time.

In preferred embodiments of the invention when used to track fiducial markers, the present invention allows for the tracking of arbitrarily shaped markers present in fluoroscopic images.

In addition to fiducial markers, the present invention can also be used to track objects of interest such as tumours and intrinsic anatomical features.

In contrast to the template-based approaches of the prior art, the present invention requires no *a priori* knowledge of the marker properties (such as shape, size and orientation) for

set up for a new patient. This obviates the requirement for imaging to be completed ahead of time in order to determine the position and orientation of the fiducial marker, thus reducing the overall quantity of radiation to which the patient is exposed during treatment. The present invention, at least in preferred embodiments, also has the advantage over template-based approaches of being a more robust solution to overlapping and arbitrarily-shaped markers.

The present invention is applicable to tumour motion tracking during external beam radiotherapy with a variety of linear accelerators, including those from Varian Medical Systems and Elektra Medical Systems.

The step of analysing may include:

generating a tracking window respectively circumscribing each object of interest by utilising a previously determined position for each fiducial marker; and

applying the convolutional neural network to the interior of each tracking window.

Preferably, the previously determined position is determined from an earlier application of the convolutional neural network. Alternatively, the previously determined position can be determined from earlier CT images of the same patient acquired prior to treatment.

Typically, the object of interest is substantially centered in the tracking window.

The position of the object of interest may be determined by:

classifying regions of the tracking window as including or not including an object of interest; and

determining the centroid of connected regions classified as including an object of interest.

Preferably, the regions are defined by traversing the tracking window with a window of smaller dimension than the tracking window.

Typically, the regions are normalised and rescaled prior to undergoing classification.

The present invention has application to the analysis of kV images and with use in image-guided radiation therapy systems.

According to some embodiments, the convolutional neural network includes three convolutional layers, two pooling layers, one fully connected layer and optionally a plurality of batch normalisation layers and rectified linear units.

The method may include the further step of identifying the target area to which radiation is to be delivered on the basis of the output object position/s.

Optionally, the method includes the further step of directing a treatment beam from the radiation therapy system based on a position of the identified target area.

The target area may be tracked by reference to successive output of object positions over time and directing the beam at the target based on said tracking. In this regard, directing the beam based on the estimated position may include adjusting or setting one or more of the following parameters of the radiation therapy system:

at least one geometrical property of said at least one emitted beam;

a position of the target relative to the beam;

a time of emission of the beam; and

an angle of emission of the beam relative to the target area about a system rotational angle.

According to another aspect of the present invention, there is provided a system for guided radiation therapy including:

a radiation source for emitting at least one treatment beam of radiation;

an imaging system arranged to generate a succession of images of a target area to which the treatment beam is to be directed; and

a control system configured to:

receive images from the imaging system;

analyse the images with a trained convolutional neural network to determine the position of one or more objects of interest present in the target area;

adjust the guided radiation therapy system to direct the treatment beam at the target area.

According to another aspect of the present invention, there is provided a computer software product comprising a sequence of instructions storable on one or more computer-readable storage media, said instructions when executed by one or more processors, cause the processor to:

receive an image from a radiation therapy system of a target area to which radiation is to be delivered;

analyse the image with a trained convolutional neural network to determine the position of one or more objects of interest present in the target area; and

output the fiducial marker position/s to the radiation therapy system.

As used herein, except where the context requires otherwise, the term "comprise" and variations of the term, such as "comprising", "comprises" and "comprised", are not intended to exclude further additives, components, integers or steps.

Further aspects of the present invention and further embodiments of the aspects described in the preceding paragraphs will become apparent from the following description, given by way of example and with reference to the accompanying drawings.

Brief description of the drawings

Figure 1 illustrates a schematic representation of a system configured to implement an embodiment of the present invention.

Figure 2 is a flowchart of a guided radiation therapy process according to an embodiment of the present invention.

Figure 2A shows various examples of markers from training and validation datasets.

Figure 2B is a schematic illustration of the CNN architectures that are suitable for practising and/or validating embodiments of the present invention.

Figure 3 illustrates an image analysis methodology performed by an embodiment of the present invention.

Figure 4A shows PRC curves on cylindrical shaped marker classification performance for full training and transfer learning approaches. (a) Full PRC curve. (b) Detailed PRC curve.

Figure 4B shows PRC curves on arbitrarily shaped marker classification performance for full training and transfer learning approaches.

Figure 4C is a graph of the mean RMSE and the 1st and 99th percentiles of the errors of CNN multiple object tracking.

Figure 5 is an illustrative example of the present invention when used to track cylindrical shaped fiducial markers throughout a radio therapy treatment fraction.

Figure 6 is an illustrative example of the present invention when used to track arbitrarily shaped fiducial markers throughout a radio therapy treatment fraction.

Detailed description of the embodiments

Figure 1, depicts a system for image guided radiation therapy able to implement an embodiment of the inventions described herein. The system 10 includes:

A radiation source 12 for emitting at least one treatment beam of radiation. The radiation source emits the treatment beam 14 along a first beam axis towards the patient being treated. Typically the radiation source 12 will comprise a linear accelerator emitting megavolt x-rays.

An imaging system 16 arranged to generate a succession of images 18 comprising a two dimensional projection of a field of view and in which the location of the target may be identified. The imaging system 16 includes a second radiation source 20 that emits at least one imaging beam 22 along a second beam axis. The imaging beam 22 will be transmitted in a direction orthogonal to the treatment beam 14. The imaging beam is transmitted through the patient (or at least through the region of the patient) to a radiation detector 24 that is configured to detect

radiation transmitted through the target. The spatial intensity of the received radiation is converted to an x-ray image that is a projection of said at least one imaging beam in a plane normal to the direction its emission. Typically, the imaging system will be a kilovolt imaging system built into the linear accelerator. In embodiments of the present invention, the imaging system is arranged to only intermittently emit its imaging beam to thereby reduce the patient's radiation exposure compared to continuous imaging. The rate of imaging can vary depending on requirements or system configuration, but will typically have an imaging interval between 0.1s to 60s. Some embodiments may have a longer imaging interval.

A support platform 26 (e.g. a bed) on which the subject of the radiation therapy is supported during treatment. Support platform 26 is repositionable relative to the imaging system and radiation source, so that the patient can be positioned with the centre of the target (i.e. tumour) located as near as possible to the intersection between the first and second beam axes.

A control system 30 that controls the parameters of operation of the radiation therapy system. Generally speaking, the control system 30 is a computer system comprising one or more processors with associated working memory, data storage and other necessary hardware, that operates under control of software instructions to receive input data from one or more of a user, other components of the system (e.g. the imaging system 16), and outputs control signals to control the operation of the radiation therapy system. Amongst other things, the control system 30 causes the radiation source 12 to direct its at least one treatment beam at the target. To do this, the control system receives images from the imaging system, analyses those images to determine the position of fiducial markers present in the target (thereby estimating the motion of the target), and then issues a control signal to adjust the system 10 to better direct the treatment beam 14 at the target.

As will be appreciated by those skilled in the art, the radiation source 12, imaging system 16 and support platform 30 are common to most conventional image radiation therapy systems. Accordingly, in the conventional manner the radiation source 12 and imaging system 16 can be rotatably mounted (on a structure commonly called a gantry) with respect to the patient support platform 30 so that they can rotate about the patient in use. The rotational axis of the gantry

motion is typically orthogonal to the directions of the treatment beam and imaging beam (i.e. the first and second directions.) This enables sequential treatment and imaging of the patient at different angular positions about the system's gantry's axis.

As noted above, the control system 30 processes images received from the imaging system 16 to estimate the motion of the target, and then issues a control signal to adjust the system 10 to better direct the treatment beam at the target. The adjustment typically comprises at least one of the following: changing a geometrical property of the treatment beam such as its shape or position, e.g. by adapting a multi-leaf collimator of the linac; changing the time of emission of the beam, e.g. by delaying treatment beam activation to a more suitable time; gating the operation of the beam, e.g. turning off the beam if the estimated motion is greater than certain parameters; changing an angle at which the beam is emitted relative to the target about the system rotational axes. The system 10 can also be adjusted so as to better direct the treatment beam at the target by moving the patient support platform 26. Moving the support platform 26 effectively changes the position of the centroid of the target with respect to the position of the treatment beam 14 (and imaging beam).

In use, the general method of operation of the system 10 is as follows. The radiation source and imaging system rotates around the patient during treatment. The imaging system acquires 2D projections of the target separated by an appropriate time interval. As discussed above, the target (tumour) will be marked by the placement of fiducial markers within or about the target. The positioning of the markers may be such that the centroid of the markers lies at the centre of the target, but this is not strictly necessary. The control system 30 uses the periodically received 2D projections (e.g. kV X-ray images) to estimate the tumour's position. The control system therefore needs a mechanism for determining the position of the fiducials and then performing ongoing estimation of the target's location and orientation in 3-dimensions.

Figure 2 illustrates a method of guided radiation therapy in which the present invention can be practiced. The methods of guided radiation therapy are similar to those followed by Huang et al. 2015 (Huang, C.-Y., Tehrani, J. N., Ng, J. A., Booth, J. T. & Keall, P. J. 2015. Six Degrees-of-Freedom Prostate and Lung Tumour Motion Measurements Using Kilovoltage Intrafraction Monitoring. Int J Radiat Oncol Biol Phys, 91, 368-375;); and Keall et al. 2016 (Keall, P. J., Ng, J. A., Juneja, P., O'brien, R. T., Huang, C.-Y., Colvill, E., Caillet, V., Simpson, E., Poulsen, P. R., Kneebone, A., Eade, T. & Booth, J. T. 2016. Real-Time 3D Image Guidance Using a Standard LINAC: Measured Motion, Accuracy, and Precision of the First Prospective

Clinical Trial of Kilovoltage Intrafraction Monitoring Guided Gating for Prostate Cancer Radiation Therapy. Int J Radiat Oncol Biol Phys, 94, 1015-1021) (the contents of which are each incorporated by reference for all purposes with the exception of the use of the motion tracking method described herein).

The process 200 can be divided into two phases, set up or the learning phase 201 and treatment 202. The learning phase 201 uses an imaging procedure 204, e.g. Cone Beam CT, before treatment to initialise 206 the parameters for a movement tracking framework. As described below, target segmentation 208 is used to identify fiducial markers in the target during initialisation. After initialisation, the method moves to the treatment phase 202. During the treatment phase the treatment beam is activated and the target irradiated, movement tracking system will update the tumour's translational and rotational motion 224 in real-time using the small-field kV images 220. As explained in more detail below, the position of the fiducial markers is identified and this data is used to check and possibly update a position estimation model.

The key component of the marker tracking system is the use of a convolutional neural network (CNN) to detect fiducial markers within kilovoltage (kV) images. The following description outlines the creation of the image datasets used for the CNN training and the network architectures. Two methods of training are described, namely training from scratch and fine-tuning using a pretrained CNN. The workflow for real-time marker tracking using the trained CNN is then described.

Training and Validation Datasets

The training of a CNN requires a large dataset of training images for it to accurately learn the required features. A separate large validation dataset is used after training to assess the accuracy of the CNN on new unseen images. The first pre-processing technique applied to both datasets was the application of a temporal filter to reduce the level of noise (including MV scatter noise). The temporal filter was performed by averaging three consecutive frames.

Each kV image of size 1024 x 768 pixels is then divided into smaller images of size 32 x 32 pixels producing 768 training images per kV image. In the case of overlapping markers, each image contained an entire marker and a secondary marker which could be partially or completely within the image. The input size of 32 x 32 pixels was selected to ensure that the largest type of

marker would be fully contained within the smaller images. Then, the smaller images were each normalised to ensure that all images were scaled to the same range, allowing for even feature distributions between all inputs. kV images were normalized using the following equation:

$$normalised\ image = \frac{image - mean(image)}{std(image)} \quad (1)$$

For training and validation of arbitrarily shaped marker CNNs, cone beam computed tomography (CBCT) projection images from ten fractions of seven lung cancer patients with implanted coiled markers were used. The CBCT images were normalized using the following equation:

$$I_N = \frac{I - Min(I)}{Max(I) - Min(I)} \quad (2)$$

The two different normalization methods were selected to ensure that the features of the markers would be emphasized for each image modality so as to improve the performance of the CNN

Equation 1 subtracts the mean of the pixel values in the original image from each individual pixel. Then each individual pixel is divided by the standard deviation of the pixel values in the original image. After normalisation, each image is rescaled to a 16-bit image. This normalisation process ensures that all images are scaled to the same range, allowing for even feature distributions between all inputs. Finally, these smaller images are labelled as a "marker" or "background" image.

Training and Validation Datasets

I - Cylindrical Shaped Marker Data

The cylindrical shaped marker CNNs were trained using intrafraction kV images from a phantom and five fractions from three prostate cancer patients undergoing radiotherapy at the Royal North Shore Hospital, Australia. The patients received either a standard fractionation treatment (80 Gy in 40 fractions) or a boosted high dose treatment (2x25 Gy + 23x2 Gy). Each of the patients and the phantom had three implanted cylindrical gold fiducial markers and two patients had overlapping markers. The phantom data had images with varying MV treatment

beam levels corresponding to dose rates of 0 monitor units per minute (MU/min), 300 MU/min and 600 MU/min. The lateral width of the phantom, representing pelvic width, was also varied with widths of 35.5 cm, 39.5 cm and 43.5 cm. For both patients and phantom image acquisition, the source to isocenter distance (SID) and source to detector distance (SDD) were set at 100 cm and 180 cm, respectively. The pixel size at the detector was 0.388x0.388 mm^2. Thus, the pixel size at isocenter was 0.216x0.216 mm^2. Three datasets were generated using the same patient data with additional phantom images of increasing levels of noise. Contrast-to-noise ratios (CNR) were used to quantify the highest level of noise in each dataset. Following pre-processing of the data, each of the three datasets consisted of 30,000 positive and 30,000 negative sub-images. The sub-images were randomly selected out of a larger dataset to balance the training sets. Dataset 1 included images with the lowest levels of noise (CNR = 1.6 ± 0.15), dataset 2 included images with moderate levels of noise (CNR = 0.33 ± 0.12) and dataset 3 included images with the highest levels of noise (CNR = 0.19 ± 0.11) (Fig. 2A (a)).

The CNNs were validated against an unseen dataset of intrafraction fluoroscopic images of prostate cancer patients. The validation dataset includes fluoroscopic intrafraction images from twelve fractions of ten patients with range of pelvic widths from 37 to 40 cm. Six of the patients received the same treatment as the patients used in the training dataset. The four other patients received a high dose treatment (6.25 Gy/fraction) for five fractions. All patients were treated with VMAT on a Varian Trilogy system. Each of the ten patients had three implanted gold fiducial markers and four patients had overlapping markers. In total and following pre-processing, the dataset contained 78,672 positive and 2,207,996 negative sub-images (Fig. 2A (b)).

II - Arbitrarily Shaped Marker Data

CBCT projection images from ten fractions of seven lung cancer patients with one to four implanted Visicoil markers were used for the training and validation of the arbitrarily shaped marker CNNs. For these images, the pixel size at isocenter is 0.259x0.259 mm2 (SDD=150 cm). The training dataset consisted of 100,000 positive and 100,000 negative sub-images derived from six fractions of three patients (Fig. 2A (c)). To create a balanced training dataset, the sub-images were randomly selected out of a larger dataset. The CNNs were validated against 115,288 positive and 1,329,562 negative sub-images from four fractions of the other four unseen patients (Fig. 2A (d)). The training and validation datasets each had eight distinct markers in total.

CNN Architectures

The automated tracking according to the invention requires a fast and accurate CNN to detect implanted fiducial markers in real time during radiotherapy. One such architecture that is suitable for practising the present invention is illustrated in Figure 2B. Various CNN models and training methods were investigated to determine the best performing model in terms of accuracy and speed of marker detection. The CNNs developed are binary classifiers that distinguish between positive images containing a marker and negativebackground images. A first CNN model used for full training consists of three convolutional layers, two pooling layers and one fully connected layer (Figure 2B (a) . Three batch normalisation layers and three rectified linear units (ReLU) were used to reduce initialisation sensitivity and accelerate the training of the CNN.

For comparison, transfer learning was performed using 'AlexNet'. AlexNet is a pretrained CNN which has been trained on over a million natural colour images. AlexNet has five convolutional layers with three pooling layers and three fully connected layers (Figure 2B (b)). Transfer learning involves the transferring of the pre-learnt features to a new application. The last fully connected layer is replaced with a new fully connected layer with two neurons for binary classification. Additional pre-processing of the training and validation datasets was required prior to being used with AlexNet since AlexNet is trained on colour images of size 227 x 277 pixels. The images in the dataset were thus required to be enlarged from 32 x 32 pixels to 227 x 277 pixels and the single grayscale channel was repeated three times to produce a 3-channel RGB image.

The CNNs were trained using the Matlab Neural Network Toolbox™ on a desktop computer with two Intel® Xeon® Gold 6130 processors (2.1 GHz) with 64 GB RAM and a NIVIDIA® Quadro® P6000 Graphics Processing Unit (GPU).A stochastic gradient descent with momentum was used to minimise the error function by updating the weights and biases. A mini-batch sizes of 128 and 256 were used for the stochastic gradient descent algorithm for the training of the cylindrical marker CNNs and arbitrarily shaped marker CNNs respectively. Each network was trained with a constant learning rate of 0.0001 and a momentum of 0.9. The datasets were shuffled before each epoch to ensure that the same data was not discarded every epoch. Early stopping regularization was employed using additional unseen images to avoid overfitting.

The use of the CNN in a radiation therapy system is described by reference to Figure 3. At step 300, after initiation of the tracking system, the initial position of the markers is defined by the user for the first kV image. The position and number of markers selected is used for the subsequent frames. At step 302, the marker positions are output to image guided radiation therapy system 10 in a suitable format to effect operational control of the system's components (principally the treatment beam and support platform 26). Typically, the data can be formatted in a suitable manner to provide three-dimensional positional information in order to effect motion of radiation therapy system' components along and about three cardinal axes.

Examples of the use of marker positions to effect operational control of the radiation therapy system include:

- estimating motion between the time of capture of individual images so as to perform tracking/targeting at a sub-imaging interval time frame; and
- use in patient set-up;

At step 304, a kV image captured by imaging system 16 during operation of the radiation therapy system 10 is received at the control system 30.

The image is analysed first by generating tracking windows using the previously determined location of the markers. A tracking window is a cropped area which is centred on each individual marker. The tracking window has been found to significantly improve the efficiency of the detection process by reducing the number of regions required to be searched. The size of each tracking window accounts for the movement of the marker in between each frame while not being too large and increasing the number of images which are required to be classified.

Each marker has a window of a set size as shown in Figure 3. The ideal tracking window size for the described embodiment is 46 x 46 pixels, as it has been found that smaller window sizes reduce the detection accuracy. Conversely, increasing the window size significantly correspondingly decreases the speed of detection, as a larger number of images are required to be classified.

The location of the tracking window is updated every frame by using the marker positions from the previous frame. Currently, the marker detection for each tracking window is

performed linearly. However, the speed of detection can by further reduced by processing all of the tracking windows at once in parallel on a CPU.

At step 308, a sliding window-based processing analysis is performed on the portions of the image bounded by each tracking window in order to determine the position of the marker. The sliding window has a size of 32 x 32 pixels so as to coincide with the input size of the trained CNN. The window begins in the top left corner and moves downwards a pixel at a time. Upon reaching the bottom of the area, the window moves horizontally one pixel and repeats the process. Each time the sliding windows moves, the selected area is cropped and processed in a similar process to training data, in that the image is first normalised using equation 1 or 2 and rescaled to a 16-bit image.

The normalised image is classified as a "marker" or "background" using the trained CNN. If the image is identified to be a "marker", it is classified as positive and if it is identified to be "background", it is classified as negative. The centre location of a positive image is recorded in a logical array to be used later to determine the marker position. This process outlined is repeated until the entire image tracking window has been searched. In the case of overlapping markers, the width of the two tracking windows is reduced as the markers approach to ensure that the approaching markers are not detected in the alternate window. Once the markers begin to separate, the tracking windows separate and gradually increase in width to the original size.

Upon the completion of the sliding window classification (step 310), the position of the marker is determined. This step proceeds by determining the centroid of connected positive regions from the sliding window classification. The calculated centroid is the position of the marker. The x- and y-coordinates of the marker are stored and the method returns to step 302, where the stored coordinates are output to the image guided radiation therapy system 10. The stored coordinates are also utilised in the next iteration of step 306 to generate tracking windows for a newly received image.

Occasionally a marker may not be detected as a result of heavy noise. In this scenario, the position of the marker is set to the previous marker position. If a marker is not detected for a large number of frames, a larger tracking window can be set to increase the search area for the marker.

The trained CNNs were evaluated by classifying all sub-images in the validation datasets as positive (marker) or negative (background). The classifications were compared to the ground truth of the annotated validation datasets. Several analysis methods were employed to determine the performance of the CNNs against unseen validation datasets. The classification performances of the CNNs were evaluated using PRC plots. PRC plots provide a prediction of future performance for classifiers validated on imbalanced datasets. A PRC plot illustrates the relationship between precision (fraction of true positive sub-images among the positive classifications) and recall (also known as sensitivity). The AUC was used to quantify the performance of the CNN where an AUC of 1 indicates perfect classification performance. Furthermore, sensitivity (SN) (fraction of actual positive sub-images that have been correctly classified) and specificity (SP) (fraction of actual negative sub-images that have been correctly classified) of the CNNs were calculated using equations 3 and 4 respectively:

$$SN = TP/TP+FN \quad (3)$$

$$SP = TN/TN+FP \quad (4)$$

where TP is true positives, TN is true negatives, FP is false positives and FN is false negatives.

Furthermore, sensitivity and specificity of the CNNs were calculated. These two analysis methods were used to determine the performance of the CNNs against unseen validation datasets.

In addition, the performance of the cylindrical shaped marker tracking system was evaluated against the ground truth and tracking results for a KIM treatment. The ground truth was constructed using the KIM tracking results and manual segmentation where KIM failed to track markers. The arbitrarily shaped marker tracking system was evaluated against manual segmentation for the ground truth and the segmentation system developed by Poulsen et al (Poulsen PR, Fledelius W, Keall PJ, et al. A method for robust segmentation of arbitrarily shaped radiopaque structures in cone-beam CT projections. *Medical Physics*. 2011;38(4):2151-2156). The construction of arbitrarily shaped marker template required manual selection of the markers in three to six projections with a large angular separation.

In this regard, the tracking system was tested on one fraction of each patient used in the validation data, with the performance of the cylindrical shaped marker tracking system being

evaluated on ten patients against the ground truth. The ground truth was constructed using the KIM tracking results and manual segmentation where the KIM segmentation was inaccurate. The arbitrarily shaped marker tracking system was evaluated on four patients against the ground truth, with the ground truth being constructed using the Poulsen segmentation system and manual segmentation for inaccurate marker positions. This system requires the manual selection of the markers in three to six projections with a large angular separation to construct the arbitrarily shape marker template. The error of tracking system was defined as the CNN detection marker centroid minus the ground truth marker centroid. The errors were calculated in the x- and y-directions and the Euclidian distance. The Euclidian distance is defined as the straight-line distance d between the ground truth and centroid determined by the CNN and is calculated using equation 5:

$$d(\mathbf{c},\mathbf{t})=\sqrt{(t_1-c_1)^2+(t_2-c_2)^2} \quad \textbf{(5)}$$

where the CNN detection marker centroid location is $\mathbf{c} = (c_1, c_2)$ and the true marker centroid location is $\mathbf{t} = (t_1, t_2)$.

The overall errors were quantified by the calculation of the mean error and the 1st and 99th percentiles of the errors. Additionally, the RMSE for each patient was determined using equation 6:

$$\text{RMSE}=\sqrt{\frac{\sum_{i=1}^{n}(C_i-T_i)^2}{n}} \quad \textbf{(6)}$$

where C is the CNN detection value, T is the true value and n is the total number of values.

The results shown in Figures 4A and 4B demonstrate that as the amount of image data used for training increases, the accuracy also increases for both the CNNs trained from scratch and fine-tuned. The trained CNNs had high accuracy with the lowest AUC equal to 0.9994 for the fully trained CNNs and 0.9993 for the transfer learning CNN. High sensitivities and specificities were also achieved for both training methods. The sensitives and specificities ranged from 98.87 to 99.42 and 97.99 to 99.32 respectively. However, no single CNN achieved both the highest sensitivity and specificity. Altering the level of noise in the training data resulted in opposite effects on the sensitivity and specificity. Increasing the level of noise for each fully trained CNN improved the sensitivity and decreased specificity. However, different effects were

observed for the transfer learning CNN. Increasing from low (dataset 1) to moderate (dataset 2) improved the sensitivity and decreased specificity. When further increasing to a high level of noise (dataset 3), the trend was the opposite. In terms of AUCs, both training methods achieved comparable results with a difference of 0.0001 between the two training methods on each of the datasets. The AUCs slightly decreased by 0.0002 when training was performed using data with higher MV scatter noise.

Figure 4A depicts PRC curves on cylindrical shaped marker classification performance for the full training and transfer learning approaches. (a) Full PRC curve. (b) Detailed PRC curve.

The following table summarises classification performance results for the cylindrical shaped marker CNNs for 78,672 positive and 2,207,996 negative samples from twelve fractions of ten patients.

Training Method	Training Dataset	Sensitivity (%)	Specificity	AUC
Full training	1	98.87	99.32	0.9996
Transfer learning	1	99.18	98.96	0.9995
Full training	2	99.00	98.92	0.9995
Transfer learning	2	99.42	98.13	0.9994
Full training	3	99.35	97.99	0.9995
Transfer learning	3	99.04	98.39	0.9995

The results for the arbitrarily shaped marker CNNs are illustrated in Figure 4B and the following Table 2. These compare the results of full training and transfer learning for arbitrarily shaped marker CNNs using a large dataset. The transfer learning CNN had the highest AUC of 0.9928 in comparison to 0.9828 for full training. Full training had a higher sensitivity of 98.58% compared to 98.49% for the transfer learning CNN. Transfer learning improved the specificity from 98.97% for full training to 99.56%. Overall, the transfer learning has better performance for arbitrarily shaped markers.

Figure 4B depicts PRC curves on arbitrarily shaped marker classification performance for full training and transfer learning approaches with Figure 4B (a) showing the full PRC curve and Figure 4B(b) showing the detailed PRC curve.

Table 2 summarises classification performance results for the arbitrarily shaped marker CNNs for 115,288 positive and 1,329,562 negative samples from four fractions of four patients.

Training Method	Sensitivity (%)	Specificity (%)	AUC
Full training	98.58	98.97	0.9828
Transfer learning	98.49	99.56	0.9928

The speed of classification of the CNNs were evaluated using a laptop system with an Intel® Core™ i7-4720HQ processor (2.60GHz) with 16 GB RAM and a NIVIDIA GeForce® GTX 970M GPU. The tracking system was implemented with a laptop system to evaluate the performance of the system on the minimum hardware that would be available. The time of classifications included the time for the rasterization and normalization of the images and CNN classification. The compact CNN performed single image classifications faster than AlexNet on a CPU and GPU. For the sliding window classification of one tracking window, AlexNet was over 16s slower than the compact CNN on a CPU. The difference in the speed of marker segmentation between the two architectures was reduced when classification was performed on a GPU.

Table 3 summarises the Table 3 summarises the mean times for the segmentation of one marker for a 46 x 46 pixel tracking window size with a step size of 2 pixels. The times are based on classifications using the cylindrical shaped marker CNNs trained on dataset 2.

CNN Architecture	Segmentation time on CPU (ms)	Segmentation time on GPU (ms)
Compact	36	9.0
AlexNet	1400	300

Following the training of the CNNs, the CNN trained from scratch on dataset 3 was used in the method described by reference to Figure 3. The errors of the tracking system for cylindrical and arbitrarily shaped markers are presented in Table 4. The arbitrarily shaped marker tracking was observed to be less accurate than the cylindrical marker tracking. The cylindrical shaped marker tracking achieved a lower mean Euclidean distance error of 1.7 ± 1.1 pixels compared to 2.9 ± 2.2 pixels for arbitrarily shaped marker tracking. The RMSE was higher in the x-direction compared to the y-direction for both types of markers (Figure. 4C). The mean error and RMSE is equivalent to sub-millimeter accuracy for both cylindrical and arbitrarily shaped marker tracking.

Table 4. Mean error, mean RMSE and the 1st and 99th percentiles of the errors of CNN multiple object tracking. The errors are calculated in the x- and y-directions and Euclidean distances for cylindrical and arbitrarily shaped markers.

	Cylindrical Shaped Marker			Arbitrarily Shaped Markers		
	X-direction	Y-direction	Euclidean Distance	X-direction	Y-direction	Euclidean Distance
Mean Error (pixels)	-0.8 ± 1.3	0.3 ± 1.2	1.7 ± 1.1	-0.9 ± 2.8	0.2 ± 2.2	2.9 ± 2.2
Mean RMSE (pixels)	1.6 ± 0.2	1.3 ± 0.4	2.0 ± 0.4	3.0 ± 0.5	2.2 ± 0.4	3.7 ± 0.5
1st Percentile (pixels)	-4.0	-3.0	0.0	-8.0	-5.0	0.0
99th Percentile (pixels)	3.0	4.0	5.4	5.0	6.0	10.0

The results presented in Fig 5 and 6 show the example tracking results for one cylindrical and one arbitrarily shaped marker respectively. The KIM system did not accurately track the cylindrical shaped marker during one treatment session of one patient (Fig. 5). For this fraction, our tracking system was able to maintain tracking throughout the fraction. Fig 5(a) shows sample kV images of the detection of a cylindrical shaped marker using the CNN tracking algorithm. Fig 5(b) and 5(c) show 2D trajectory in the x- and y-direction of the marker using the CNN tracking in comparison to the ground truth and KIM treatment tracking, respectively. Fig 5(d) shows the

error between the CNN tracking and the ground truth. (e) Error between KIM treatment tracking and the ground truth.

Fig 6. (a) shows sample CBCT projections of the detection of an arbitrarily shaped Visicoil marker using the CNN tracking algorithm. The 2D trajectory (x direction) is shown in Fig 5 (b), with the y-direction of the marker using the CNN tracking in comparison to the ground truth and Poulsen algorithm, being shown in Fig 6 (c). The error between the CNN tracking and the ground truth is shown in Fig 6(d) and the error between Poulsen et al. algorithm and ground truth shown in Fig 6(e).

It will be realized that the fully trained CNN was successfully used in a real-time multiple object tracking system that can be applied to intrafraction monitoring applications. Figures 5 and 6, and Table 4 demonstrate initial tests of the CNNs in a simple tracking system to track markers with gantry rotation. The cylindrical and arbitrarily shaped markers were successfully tracked throughout the treatment fractions. Sub-millimeter accuracy was achieved for all three cylindrical and two arbitrarily shaped marker CNNs.

The high accuracy for the detection and tracking of arbitrarily shaped markers shows the potential to track other types of markers such as liquid markers. Furthermore, the present invention can be applied to track the tumor itself, removing the need for implanted markers. This would eliminate the cost and discomfort of the marker implantation and would allow radiotherapy to commence without the delay of the marker implantation procedure. The deep-learning framework according to the invention could also be expanded to tracking abdominal markers in the liver, pancreas and kidneys since the motion within the training set does not affect the performance. This approach could also be used in a hybrid system where the CNN is used to augment template-based segmentation by optimizing the position and size of the search area.

It will be understood that the invention disclosed and defined in this specification extends to all alternative combinations of two or more of the individual features mentioned or evident from the text or drawings. All of these different combinations constitute various alternative aspects of the invention.

CLAIMS

1. A method for guiding a radiation therapy system, comprising:

capturing an image of a target area to which radiation is to be delivered;

analysing the image with a trained convolutional neural network to determine the position of one or more objects of interest present in the target area; and

outputting the determined position/s to the radiation therapy system.

2. A method according to claim 1, wherein the step of analysing includes:

generating a tracking window respectively circumscribing each object of interest by utilising a previously determined position for each object of interest; and

applying the convolutional neural network to the interior of each tracking window.

3. A method according to claim 2, wherein the previously determined position is determined from an earlier application of the convolutional neural network.

4. A method according to claim 2 or claim 3, wherein the object of interest is substantially centered in the tracking window.

5. A method according to any one of claims 2 to 5, wherein the position of the object of interest is determined by:

classifying regions of the tracking window as including or not including an object of interest; and

determining the centroid of connected regions classified as including an object of interest.

6. A method according to claim 5, wherein the regions are defined by traversing the tracking window with a window of smaller dimension than the tracking window.

7. A method according to claim 6, further including the step of reducing a dimension of a tracking window in accordance with the smaller dimension window's traversal of the tracking window.

8. A method according to claim 6 or claim 7, wherein the regions are normalised and rescaled prior to undergoing classification.

9. A method according to any preceding claim, wherein the objects of interest include a fiducial marker, tumour and intrinsic anatomical features.

10. A method according to any preceding claim, wherein the image is an x-ray image.

11. A method according to any preceding claim, wherein the radiation therapy system is a real-time image-guided radiation therapy system.

12. A method according to any preceding claim, wherein the convolutional neural network includes three convolutional layers, two pooling layers, one fully connected layer and optionally a plurality of batch normalisation layers and rectified linear units.

13. A method according to any preceding claim, further including the step of:

identifying the target area to which radiation is to be delivered on the basis of the outputted position/s.

14. A method as claimed in claim 13, further including the step of:

directing a treatment beam from the radiation therapy system based on a position of the identified target area.

15. The method of claim 14, further including the steps of:

tracking the target area by reference to successive output of positions over time; and

directing the beam at the target based on said tracking.

16. The method of either of claims 14 or 15, wherein directing the beam based on the estimated position includes adjusting or setting one or more of the following parameters of the radiation therapy system:

at least one geometrical property of said at least one emitted beam;

a position of the target relative to the beam;

a time of emission of the beam; and

an angle of emission of the beam relative to the target area about a system rotational angle.

17. A system for guided radiation therapy including:

a radiation source for emitting at least one treatment beam of radiation;

an imaging system arranged to generate a succession of images of a target area to which the treatment beam is to be directed; and

a control system configured to:

receive images from the imaging system;

analyse the images with a trained convolutional neural network to determine the position of one or more objects of interest present in the target area; and

adjust the guided radiation therapy system using the determined positions to direct the treatment beam at the target area.

18. A computer software product comprising a sequence of instructions storable on one or more computer-readable storage media, said instructions when executed by one or more processors, cause the processor to:

receive an image from a radiation therapy system of a target area to which radiation is to be delivered;

analyse the image with a trained convolutional neural network to determine the position of one or more objects of interest present in the target area; and

output the determined position/s to the radiation therapy system.

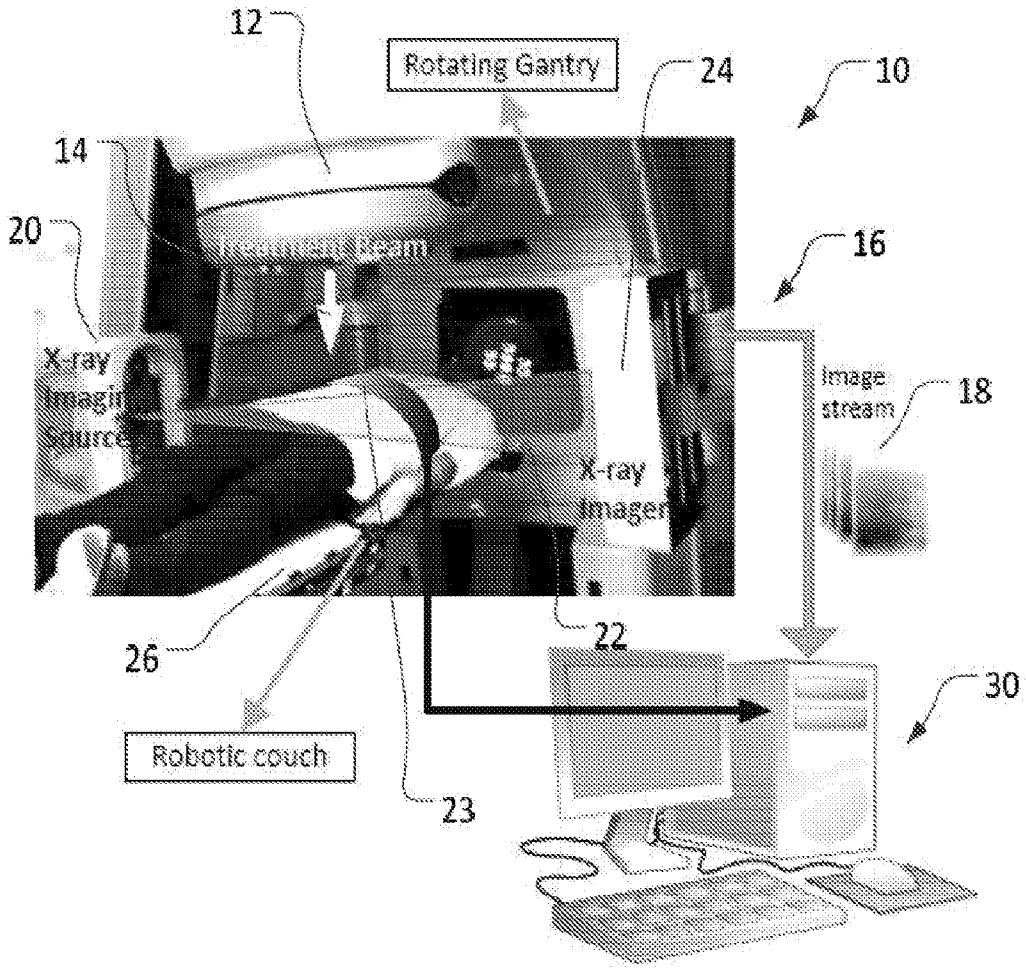
12
Rotating Gantry
24
10
14
20
16
X-ray
Imagi
Source
X-ray
Imager
Image
stream
18
22
26
30
Robotic couch
23

FIGURE 1

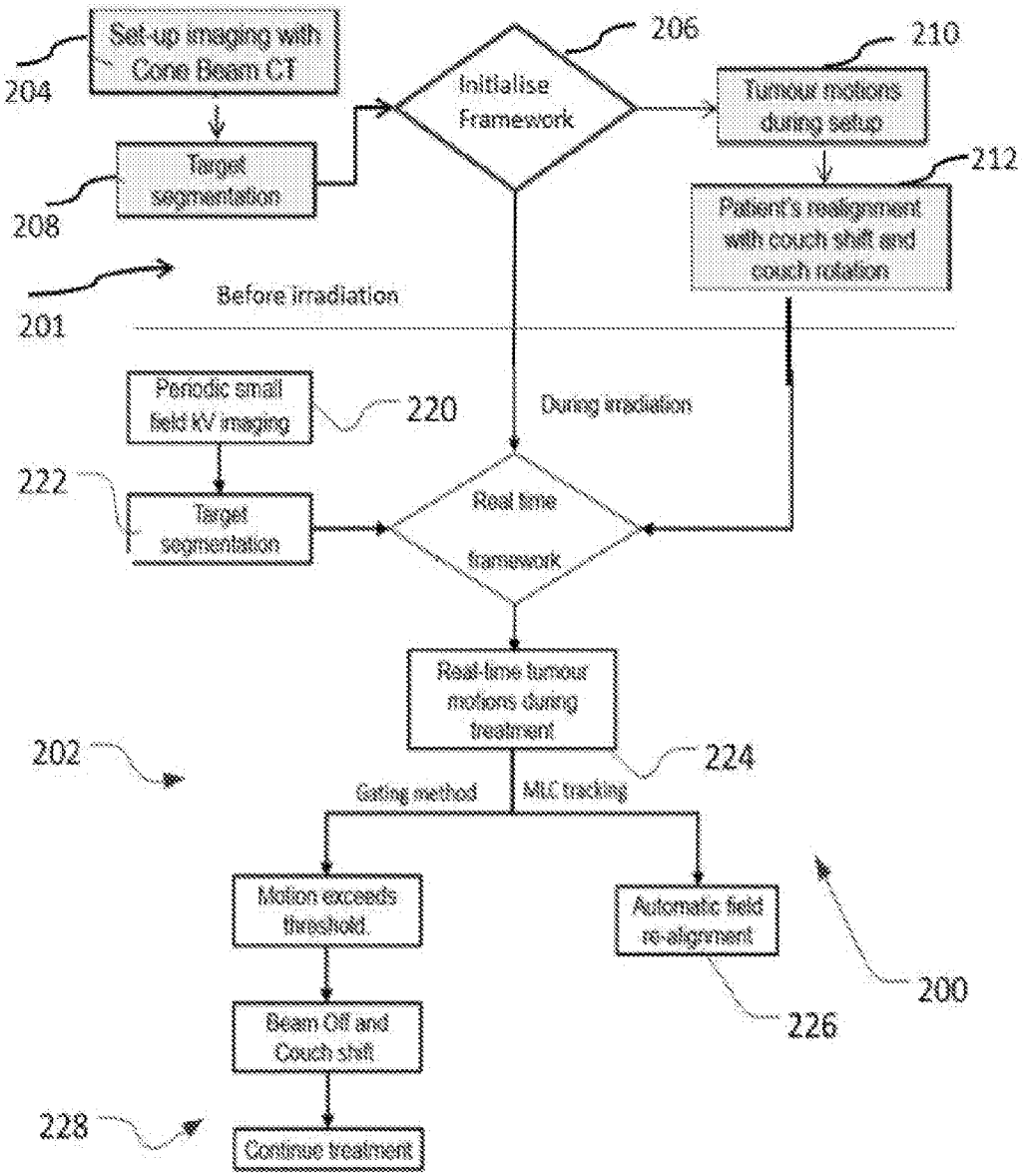
Set-up imaging with Cone Beam CT
204
Target segmentation
208
Initialise Framework
206
Tumour motions during setup
210
Patient's realignment with couch shift and couch rotation
212
201
Before irradiation
During irradiation
Periodic small field kV imaging
220
222
Target segmentation
Real time framework
Real-time tumour motions during treatment
224
202
Gating method
MLC tracking
Motion exceeds threshold
Automatic field re-alignment
200
226
Beam Off and Couch shift
228
Continue treatment

FIGURE 2

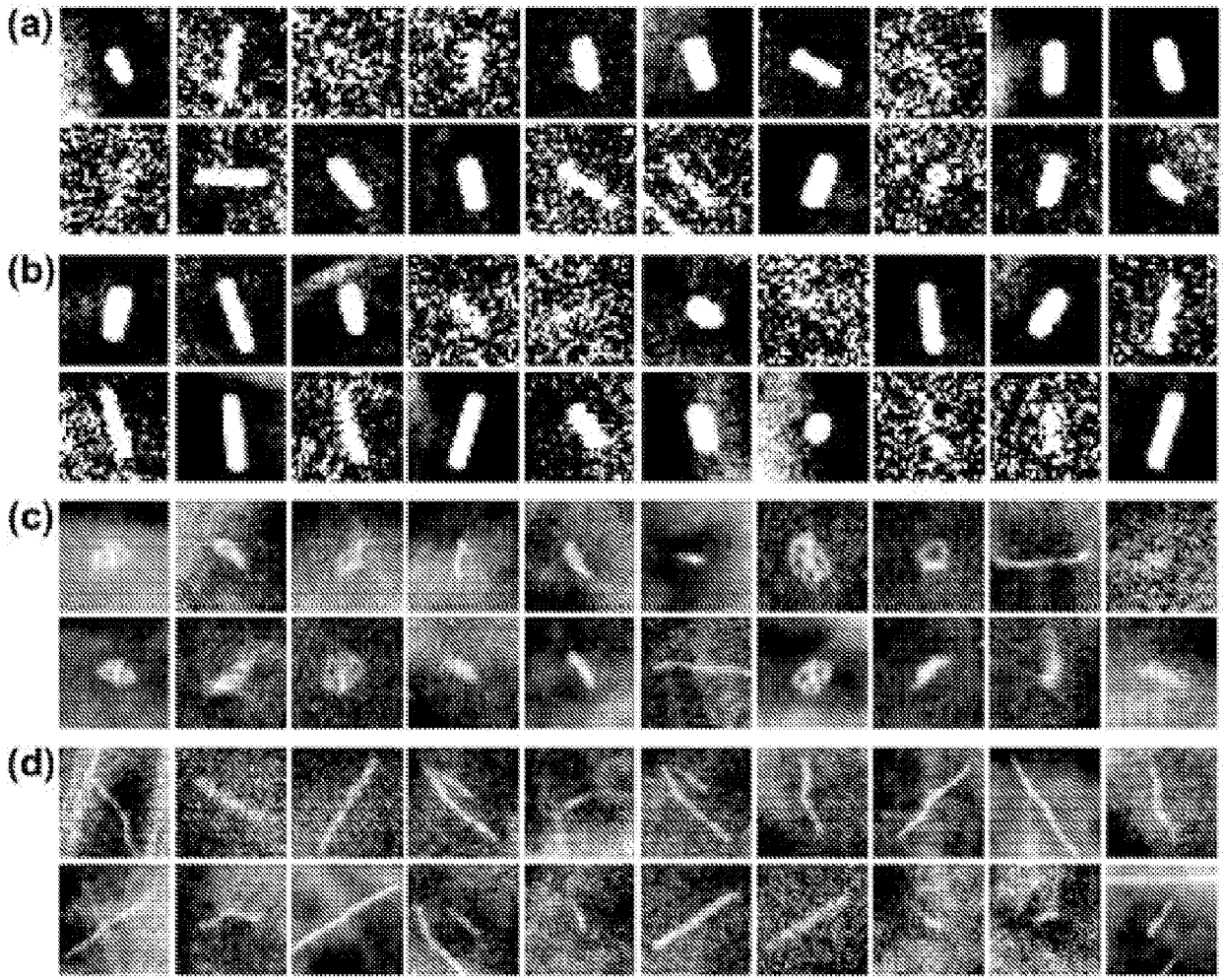

FIGURE 2A

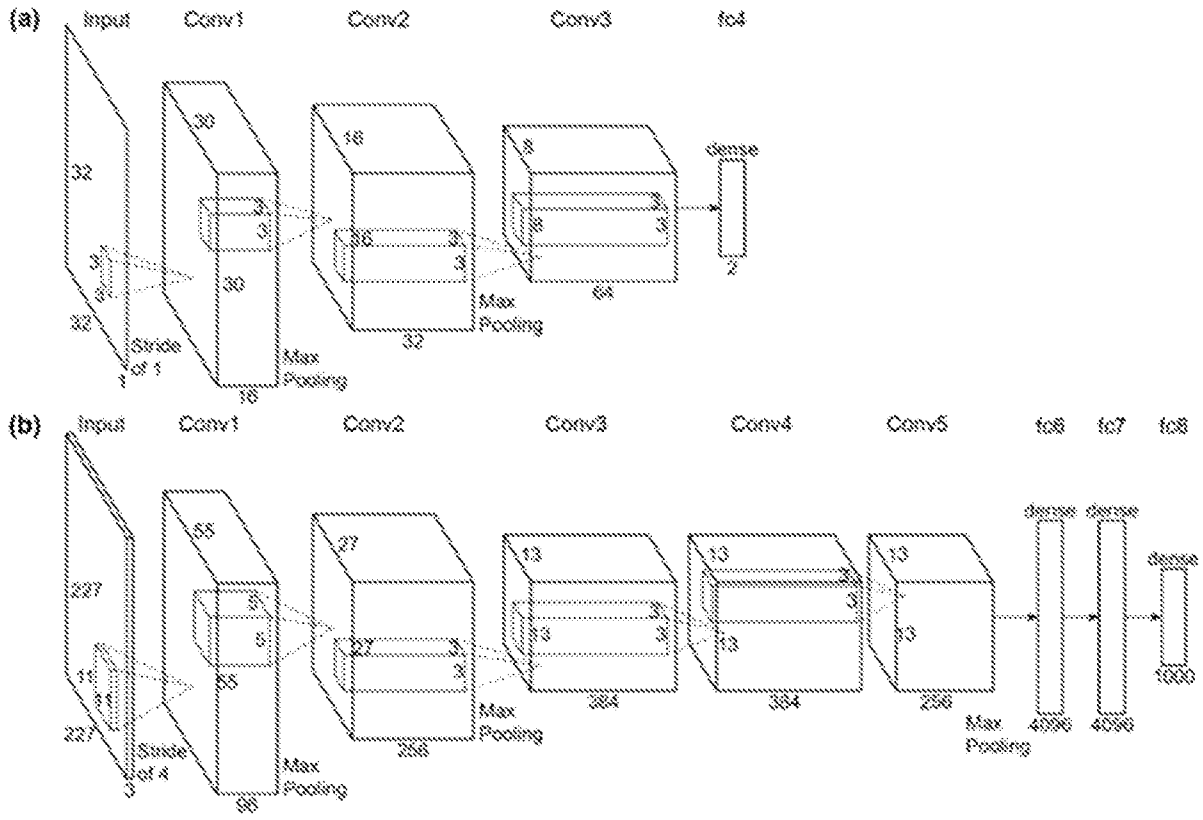
(a)
Input
Conv1
Conv2
Conv3
fc4
32
30
16
8
Dense
2
Stride of 1
Max Pooling
(b)
Input
Conv1
Conv2
Conv3
Conv4
Conv5
fc6
fc7
fc8
227
55
27
13
Stride of 4
Max Pooling
Dense
4096
1000

FIGURE 2B

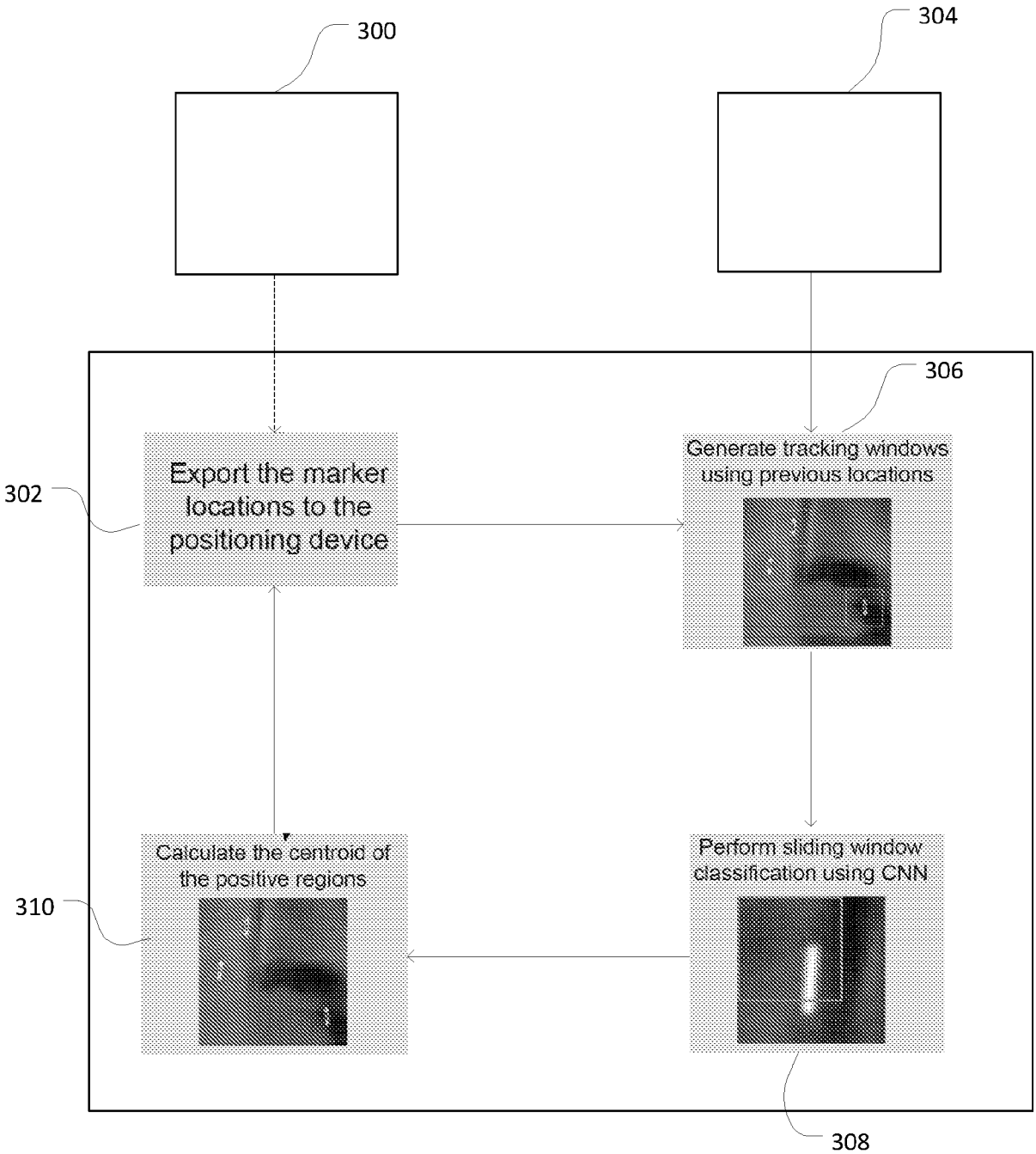
300
304
306
Export the marker locations to the positioning device
302
Generate tracking windows using previous locations
Calculate the centroid of the positive regions
310
Perform sliding window classification using CNN
308

FIGURE 3

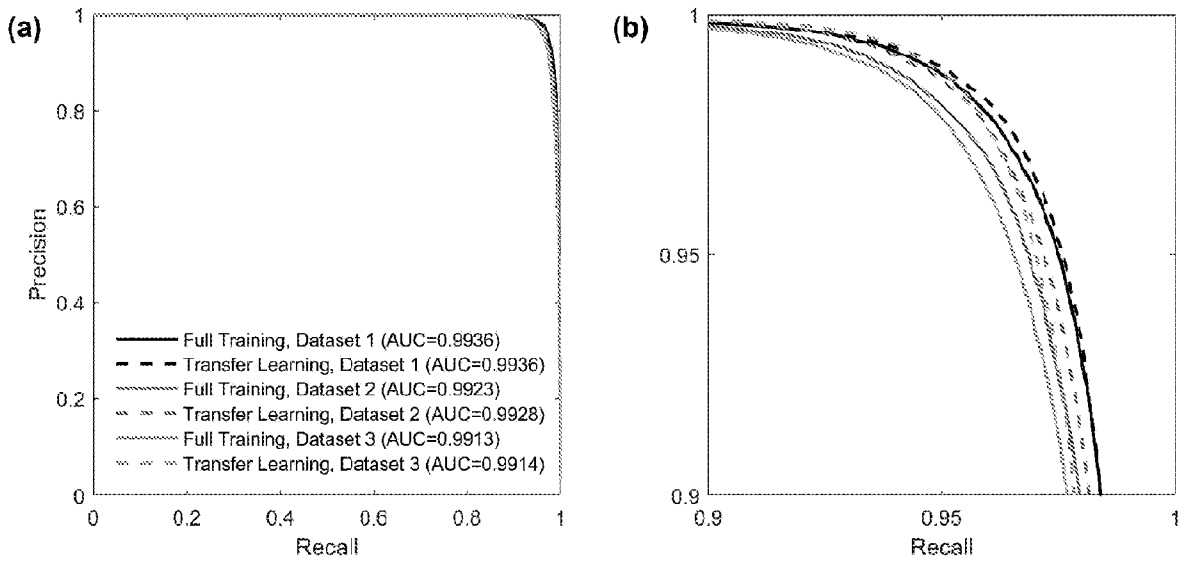

FIGURE 4A

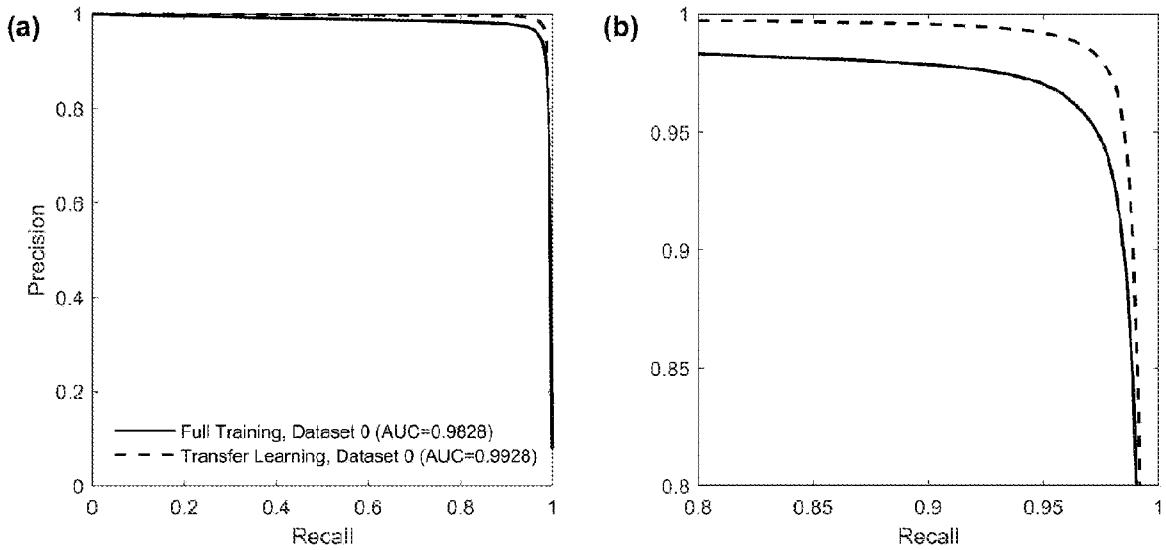

FIGURE 4B

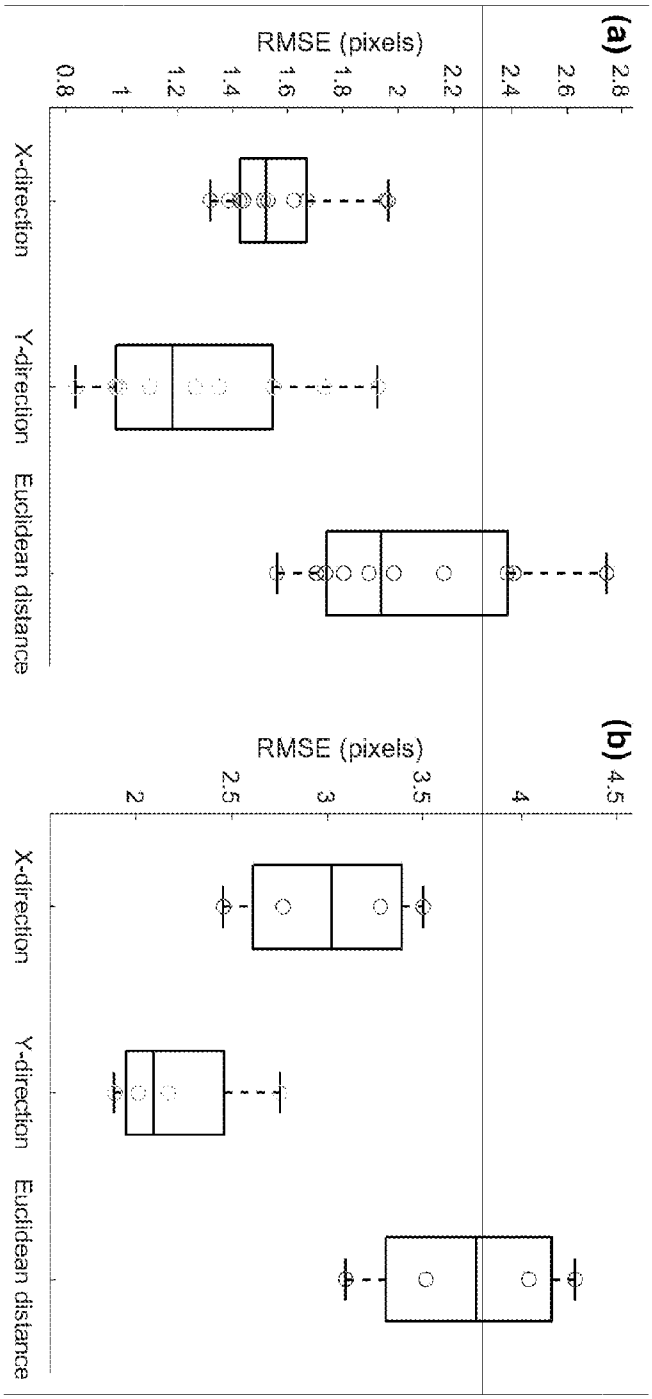
(a)
RMSE (pixels)
0.8
1
1.2
1.4
1.6
1.8
2
2.2
2.4
2.6
2.8
X-direction
Y-direction
Euclidean distance
(b)
RMSE (pixels)
2
2.5
3
3.5
4
4.5
X-direction
Y-direction
Euclidean distance

FIGURE 4C

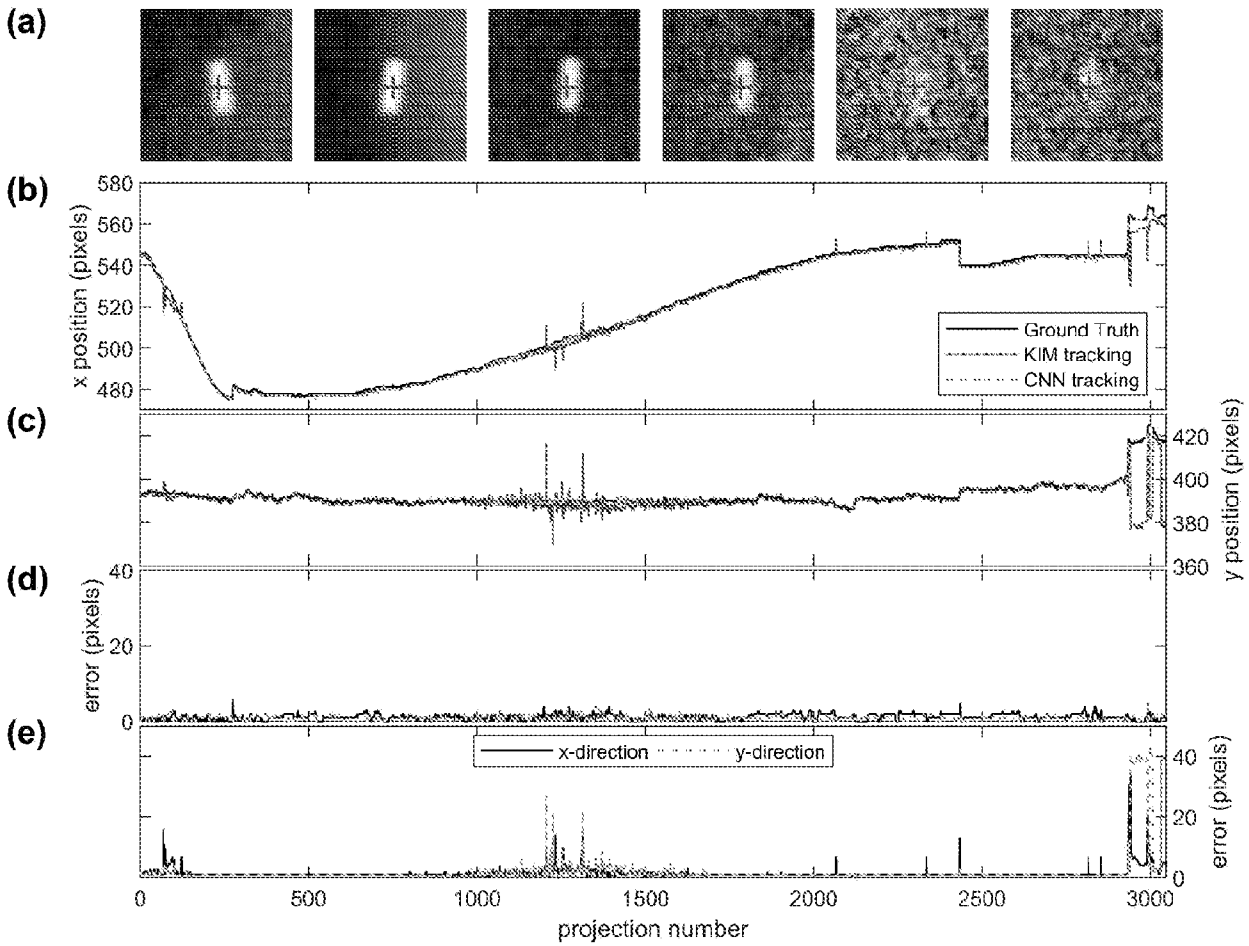
(a)
(b)
(c)
(d)
(e)
x position (pixels)
580
560
540
520
500
480
Ground Truth
KIM tracking
CNN tracking
y position (pixels)
420
400
380
360
error (pixels)
40
20
0
x-direction
y-direction
0
500
1000
1500
2000
2500
3000
projection number

FIGURE 5

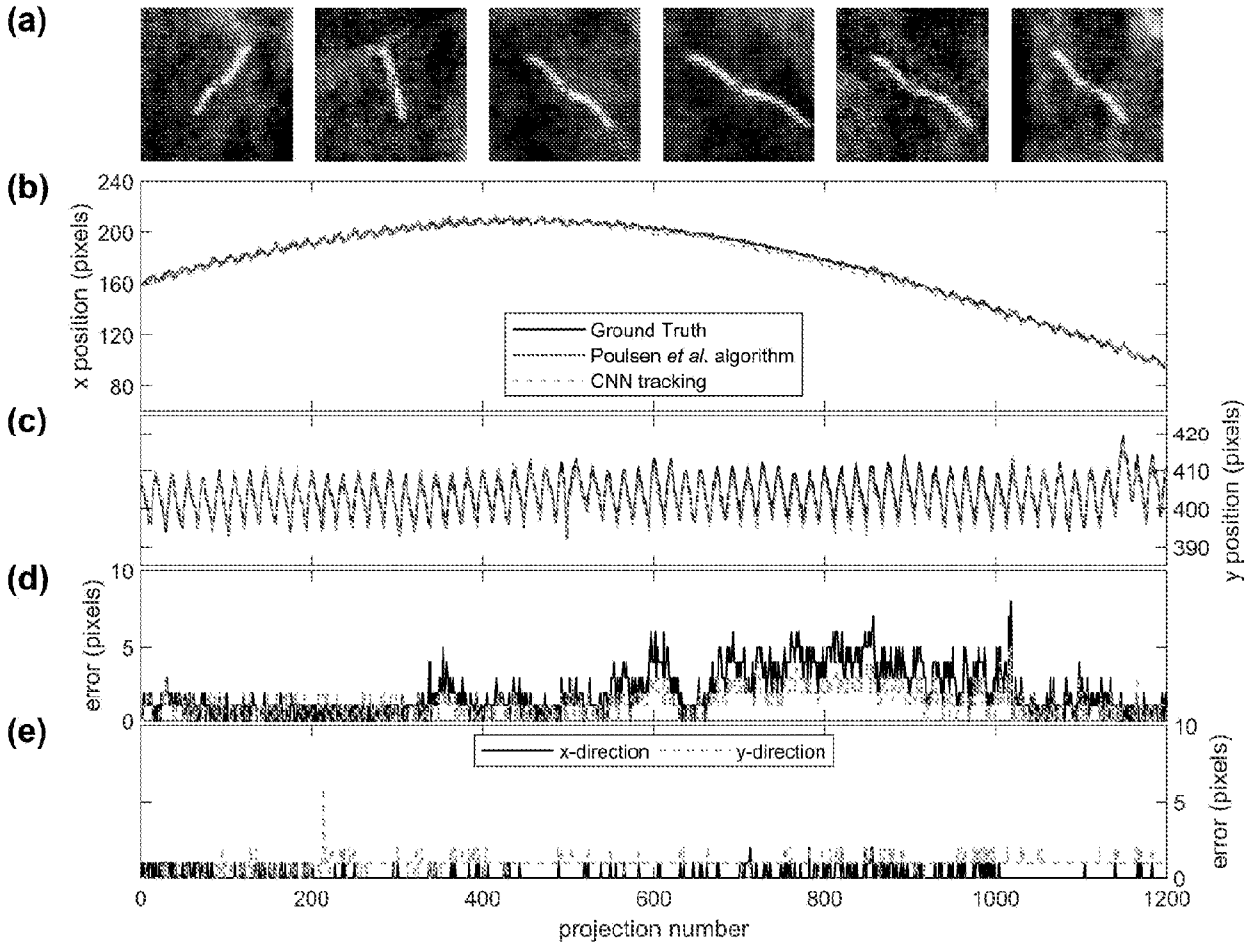
(a)
(b)
(c)
(d)
(e)
x position (pixels)
240
200
160
120
80
Ground Truth
Poulsen et al. algorithm
CNN tracking
y position (pixels)
420
410
400
390
error (pixels)
10
5
0
x-direction
y-direction
0
200
400
600
800
1000
1200
projection number

FIGURE 6

INTERNATIONAL SEARCH REPORT

International application No.
PCT/AU2019/050212

A. CLASSIFICATION OF SUBJECT MATTER

G06N 3/02 (2006.01) G06T 7/73 (2017.01) A61N 5/00 (2006.01) A61B 6/00 (2006.01)

According to International Patent Classification (IPC) or to both national classification and IPC

B. FIELDS SEARCHED

Minimum documentation searched (classification system followed by classification symbols)

Documentation searched other than minimum documentation to the extent that such documents are included in the fields searched

Electronic data base consulted during the international search (name of data base and, where practicable, search terms used)

PATENW: Classmarks IPC & CPC (various marks in A61N, A61B, G16H, G06T, G06N,G06K); Keywords (machine learning, artificial intelligence, neural w network, ANN, deep learning, convolution, CNN, DCNN, plan, control, direct, update, focus, strategy, automated, guided, radiation, therapy, image, analysis, target, object, region, zone, window, tumour, target, fiducial, marker, scan and like terms)

Google/Google Patents/ Google Scholar/ The Lens websites: Keywords (image analysis trained convolutional neural network, radiation therapy planning neural network, control radiation therapy artificial intelligence, convolutional neural network tracking window and like terms)

Applicant(s)/Inventor(s) name search: Google Patents websites, AUSPAT and internal databases provided by IP Australia

C. DOCUMENTS CONSIDERED TO BE RELEVANT

Category*	Citation of document, with indication, where appropriate, of the relevant passages	Relevant to claim No.
	Documents are listed in the continuation of Box C	

[X] Further documents are listed in the continuation of Box C [X] See patent family annex

* Special categories of cited documents:

"A" document defining the general state of the art which is not considered to be of particular relevance

"E" earlier application or patent but published on or after the international filing date

"L" document which may throw doubts on priority claim(s) or which is cited to establish the publication date of another citation or other special reason (as specified)

"O" document referring to an oral disclosure, use, exhibition or other means

"P" document published prior to the international filing date but later than the priority date claimed

"T" later document published after the international filing date or priority date and not in conflict with the application but cited to understand the principle or theory underlying the invention

"X" document of particular relevance; the claimed invention cannot be considered novel or cannot be considered to involve an inventive step when the document is taken alone

"Y" document of particular relevance; the claimed invention cannot be considered to involve an inventive step when the document is combined with one or more other such documents, such combination being obvious to a person skilled in the art

"&" document member of the same patent family

Date of the actual completion of the international search	Date of mailing of the international search report
20 May 2019	20 May 2019

Name and mailing address of the ISA/AU

AUSTRALIAN PATENT OFFICE
PO BOX 200, WODEN ACT 2606, AUSTRALIA
Email address: pct@ipaustralia.gov.au

Authorised officer

Neil Miller
AUSTRALIAN PATENT OFFICE
(ISO 9001 Quality Certified Service)
Telephone No. +61262104089

INTERNATIONAL SEARCH REPORT C (Continuation). DOCUMENTS CONSIDERED TO BE RELEVANT		International application No. **PCT/AU2019/050212**
Category*	Citation of document, with indication, where appropriate, of the relevant passages	Relevant to claim No.
Y	US 2016/0174902 A1 (SIEMENS AKTIENGESELLSCHAFT) 23 June 2016 paras [0036], [0039], [0050], [0061]-[0068], [0074], [0094], [0130], Figs 2, 3, 5, 9-11, 14, 21, 22 and 24	1-18
Y	US 7643661 B2 (RUCHALA et al.) 05 January 2010 Col. 8 line 18-Col. 11 line 3, Figs 5-7	1-18
A	Liu, Y. et al. "A deep convolutional neural network-based automatic delineation strategy for multiple brain metastases stereotactic radiosurgery." PloS one 12. no.10: e0185844. 6 October 2017 Whole Document	1-18
A	WO 2016/144914 A1 (DUKE UNIVERSITY) 15 September 2016 Whole document	1-18
A	Krizhevsky, A. et al. "Imagenet classification with deep convolutional neural networks." Advances in neural information processing systems. 2012. Whole document	1-18
T	Meyer, P. et al. "Survey on deep learning for radiotherapy." Computers in Biology and Medicine 98 (2018) pp.126-146. sections 1, 2, 3.1-3.6	1,17 and 18
P,X	WO 2019/027924 A1 (ICAHN SCHOOL OF MEDICINE AT MOUNT SINAI) 07 February 2019 paras [0022]-[0068] Figs 1, 2 and 3	1, 17 and 18
P,X	US 2019/0030371 A1 (ELEKTA, Inc) 31 January 2019 paras [0027]-[0102], Figs 2-10	1, 17 and 18

INTERNATIONAL SEARCH REPORT Information on patent family members	International application No. **PCT/AU2019/050212**

This Annex lists known patent family members relating to the patent documents cited in the above-mentioned international search report. The Australian Patent Office is in no way liable for these particulars which are merely given for the purpose of information.

Patent Document/s Cited in Search Report		Patent Family Member/s	
Publication Number	**Publication Date**	**Publication Number**	**Publication Date**
US 2016/0174902 A1	23 June 2016	US 2016174902 A1	23 Jun 2016
		US 9730643 B2	15 Aug 2017
		CN 106408610 A	15 Feb 2017
		CN 106456078 A	22 Feb 2017
		EP 3057510 A1	24 Aug 2016
		EP 3057510 B1	28 Nov 2018
		EP 3093821 A1	16 Nov 2016
		EP 3461414 A1	03 Apr 2019
		US 2016106321 A1	21 Apr 2016
		US 9538925 B2	10 Jan 2017
		US 2015065864 A1	05 Mar 2015
		US 9629563 B2	25 Apr 2017
		US 2015238148 A1	27 Aug 2015
		US 9668699 B2	06 Jun 2017
		US 2015112182 A1	23 Apr 2015
		US 9700219 B2	11 Jul 2017
		US 2017265754 A1	21 Sep 2017
		US 9974454 B2	22 May 2018
		US 2018242857 A1	30 Aug 2018
		US 10258244 B2	16 Apr 2019
		WO 2015058044 A1	23 Apr 2015
US 7643661 B2	05 January 2010	US 2007041494 A1	22 Feb 2007
		US 7643661 B2	05 Jan 2010
		AU 2006272730 A1	01 Feb 2007
		AU 2006272742 A1	01 Feb 2007
		AU 2006272746 A1	01 Feb 2007
		AU 2006302865 A1	26 Apr 2007
		CA 2616136 A1	01 Feb 2007
		CA 2616138 A1	01 Feb 2007
		CA 2616272 A1	01 Feb 2007
		CA 2616292 A1	01 Feb 2007
		CA 2616296 A1	01 Feb 2007
		CA 2616299 A1	01 Feb 2007
		CA 2616301 A1	01 Feb 2007
		CA 2616304 A1	01 Feb 2007

Due to data integration issues this family listing may not include 10 digit Australian applications filed since May 2001.

INTERNATIONAL SEARCH REPORT Information on patent family members	International application No. **PCT/AU2019/050212**

This Annex lists known patent family members relating to the patent documents cited in the above-mentioned international search report. The Australian Patent Office is in no way liable for these particulars which are merely given for the purpose of information.

Patent Document/s Cited in Search Report		Patent Family Member/s	
Publication Number	**Publication Date**	**Publication Number**	**Publication Date**
		CA 2616306 A1	01 Feb 2007
		CA 2616309 A1	01 Feb 2007
		CA 2616316 A1	01 Feb 2007
		CA 2625368 A1	26 Apr 2007
		CN 101267768 A	17 Sep 2008
		CN 101267769 A	17 Sep 2008
		CN 101267770 A	17 Sep 2008
		CN 101267857 A	17 Sep 2008
		CN 101267858 A	17 Sep 2008
		CN 101268467 A	17 Sep 2008
		CN 101268467 B	18 Jul 2012
		CN 101268474 A	17 Sep 2008
		CN 101268476 A	17 Sep 2008
		CN 101500648 A	05 Aug 2009
		CN 101500648 B	04 Jul 2012
		CN 101505652 A	12 Aug 2009
		CN 101512547 A	19 Aug 2009
		CN 101529442 A	09 Sep 2009
		EP 1906826 A2	09 Apr 2008
		EP 1906827 A2	09 Apr 2008
		EP 1906828 A2	09 Apr 2008
		EP 1907058 A2	09 Apr 2008
		EP 1907058 B1	24 Jun 2015
		EP 1907059 A2	09 Apr 2008
		EP 1907064 A2	09 Apr 2008
		EP 1907064 B1	08 Jun 2011
		EP 1907065 A2	09 Apr 2008
		EP 1907065 B1	07 Nov 2012
		EP 1907066 A2	09 Apr 2008
		EP 1907968 A2	09 Apr 2008
		EP 1907981 A2	09 Apr 2008
		EP 1907984 A2	09 Apr 2008
		EP 1934898 A2	25 Jun 2008
		EP 1970097 A2	17 Sep 2008
		EP 1977788 A2	08 Oct 2008
		EP 1977788 B1	04 May 2011

Due to data integration issues this family listing may not include 10 digit Australian applications filed since May 2001.

INTERNATIONAL SEARCH REPORT Information on patent family members	International application No. **PCT/AU2019/050212**

This Annex lists known patent family members relating to the patent documents cited in the above-mentioned international search report. The Australian Patent Office is in no way liable for these particulars which are merely given for the purpose of information.

Patent Document/s Cited in Search Report		Patent Family Member/s	
Publication Number	**Publication Date**	**Publication Number**	**Publication Date**
		EP 2532386 A2	12 Dec 2012
		JP 2009502245 A	29 Jan 2009
		JP 5060476 B2	31 Oct 2012
		JP 2009502250 A	29 Jan 2009
		JP 2009502251 A	29 Jan 2009
		JP 2009502252 A	29 Jan 2009
		JP 2009502253 A	29 Jan 2009
		JP 2009502254 A	29 Jan 2009
		JP 2009502255 A	29 Jan 2009
		JP 2009502257 A	29 Jan 2009
		JP 2009506800 A	19 Feb 2009
		JP 2009507524 A	26 Feb 2009
		JP 2009511164 A	19 Mar 2009
		JP 2009514559 A	09 Apr 2009
		KR 20080039916 A	07 May 2008
		KR 20080039919 A	07 May 2008
		KR 20080039920 A	07 May 2008
		KR 20080039924 A	07 May 2008
		KR 20080039925 A	07 May 2008
		KR 20080039926 A	07 May 2008
		KR 20080044247 A	20 May 2008
		KR 20080044249 A	20 May 2008
		KR 20080044251 A	20 May 2008
		KR 20080044252 A	20 May 2008
		KR 20080049716 A	04 Jun 2008
		KR 20080057265 A	24 Jun 2008
		TW 200722133 A	16 Jun 2007
		TW 200722134 A	16 Jun 2007
		TW 200722135 A	16 Jun 2007
		TW 200722136 A	16 Jun 2007
		TW 200722137 A	16 Jun 2007
		TW 200724187 A	01 Jul 2007
		TW 200724188 A	01 Jul 2007
		TW 200724189 A	01 Jul 2007
		TW 200724191 A	01 Jul 2007
		TW 200724192 A	01 Jul 2007

Due to data integration issues this family listing may not include 10 digit Australian applications filed since May 2001.

INTERNATIONAL SEARCH REPORT Information on patent family members	International application No. **PCT/AU2019/050212**

This Annex lists known patent family members relating to the patent documents cited in the above-mentioned international search report. The Australian Patent Office is in no way liable for these particulars which are merely given for the purpose of information.

Patent Document/s Cited in Search Report		Patent Family Member/s	
Publication Number	**Publication Date**	**Publication Number**	**Publication Date**
		TW 200726500 A	16 Jul 2007
		TW 200730211 A	16 Aug 2007
		US 2007189591 A1	16 Aug 2007
		US 7567694 B2	28 Jul 2009
		US 2007043286 A1	22 Feb 2007
		US 7574251 B2	11 Aug 2009
		US 2007195930 A1	23 Aug 2007
		US 7609809 B2	27 Oct 2009
		US 2007041495 A1	22 Feb 2007
		US 7639853 B2	29 Dec 2009
		US 2007041497 A1	22 Feb 2007
		US 7639854 B2	29 Dec 2009
		US 2007041499 A1	22 Feb 2007
		US 7773788 B2	10 Aug 2010
		US 2007195929 A1	23 Aug 2007
		US 7839972 B2	23 Nov 2010
		US 2007201613 A1	30 Aug 2007
		US 8229068 B2	24 Jul 2012
		US 2011112351 A1	12 May 2011
		US 8442287 B2	14 May 2013
		US 2007076846 A1	05 Apr 2007
		US 8767917 B2	01 Jul 2014
		US 2007088573 A1	19 Apr 2007
		US 2007195922 A1	23 Aug 2007
		WO 2007014026 A2	01 Feb 2007
		WO 2007014091 A2	01 Feb 2007
		WO 2007014092 A2	01 Feb 2007
		WO 2007014093 A2	01 Feb 2007
		WO 2007014094 A2	01 Feb 2007
		WO 2007014104 A2	01 Feb 2007
		WO 2007014105 A2	01 Feb 2007
		WO 2007014106 A2	01 Feb 2007
		WO 2007014107 A2	01 Feb 2007
		WO 2007014108 A2	01 Feb 2007
		WO 2007014110 A2	01 Feb 2007
		WO 2007046910 A2	26 Apr 2007

Due to data integration issues this family listing may not include 10 digit Australian applications filed since May 2001.

INTERNATIONAL SEARCH REPORT Information on patent family members	International application No. **PCT/AU2019/050212**

This Annex lists known patent family members relating to the patent documents cited in the above-mentioned international search report. The Australian Patent Office is in no way liable for these particulars which are merely given for the purpose of information.

Patent Document/s Cited in Search Report		Patent Family Member/s	
Publication Number	**Publication Date**	**Publication Number**	**Publication Date**
		WO 2012021530 A2	16 Feb 2012
WO 2016/144914 A1	15 September 2016	WO 2016144914 A1	15 Sep 2016
		US 2018043182 A1	15 Feb 2018
WO 2019/027924 A1	07 February 2019	WO 2019027924 A1	07 Feb 2019
US 2019/0030371 A1	31 January 2019	US 2019030371 A1	31 Jan 2019

End of Annex

Due to data integration issues this family listing may not include 10 digit Australian applications filed since May 2001.